KSÜ Mühendislik Bilimleri Dergisi, 28(3), 2025
Araştırma Makalesi

KSU J Eng Sci, 28(3), 2025
Research Article

Kahramanmaras Sutcu Imam University
Journal of Engineering Sciences

Geliş Tarihi : 22.02.2025
Kabul Tarihi : 04.03.2025

Received Date : 22.02.2025
Accepted Date : 04.03.2025

ZnO STRUCTURES: THE ROLE OF MORPHOLOGY IN PHOTOCATALYTIC DEGRADATION OF REACTIVE RED-194 DYE

ZnO YAPILARI: REAKTİF KIRMIZI 194 BOYASININ FOTOKATALİTİK DEGRADASYONUNDA MORFOLOJİNİN ETKİSİ

Nazli TURKTEN[1] (ORCID: 0000-0001-9343-3697)
Yunus KARATAS[1*] (ORCID: 0000-0002-3826-463X)

[1] Department of Chemistry, Kirsehir Ahi Evran University, 40100, Kirsehir, Türkiye

*Sorumlu Yazar / Corresponding Author: Yunus KARATAS, ykaratas@ahievran.edu.tr

ABSTRACT

ZnO structures are accessible photocatalysts that can be synthesized using significantly cheaper resources than other catalyst alternatives, addressing current environmental concerns. The present research proposed a design and synthesis of ZnO structures with two different morphologies, namely flower-like ZnO (ZnO-F) and rod-like ZnO (ZnO-R) using a simple hydrothermal method. These efficient catalysts were characterized using FTIR, Raman spectroscopy, XRD, SEM, BET, and XPS analyses. Both synthesis routes resulted in the formation of wurtzite crystalline ZnO. The variation in the synthesis route affected the morphology, crystallite size, and surface area of the ZnO structures. The crystallite sizes of ZnO-F and ZnO-R specimens were 24.46 nm and 31.10 nm, respectively. SEM indicated remarkable alterations in the morphology of ZnO structures. The surface area of ZnO-F (20 m^2/g) was almost doubled compared to ZnO-R specimen (9.5 m^2/g). XPS analysis confirmed the chemical states of ZnO structures. The impact of morphology and reaction conditions on the photoactivity of ZnO structures was tested on the degradation of Reactive Red 194 (RR-194) dye and ZnO-F specimen exhibited an improved photocatalytic performance than ZnO-R.

Keywords: Flower-like, hydrothermal method, photocatalysis, photocatalytic performance, Reactive Red-194, rod-like, ZnO structures.

ÖZET

ZnO yapıları, çevre sorunlarında kullanılabilecek etkin ve ekonomik katalizörler olarak günümüzde dikkat çekmektedir. Bu çalışmada, basit bir hidrotermal yöntem kullanılarak çiçek benzeri ZnO (ZnO-F) ve çubuk benzeri ZnO (ZnO-R) olmak üzere iki farklı morfolojide ZnO yapılarının tasarımını ve sentezini önerilmiştir. Bu etkin katalizörlerin karakterizasyonu FTIR, Raman spektroskopisi, XRD, SEM, BET ve XPS analizleri ile yapılmıştır. Her iki yöntem ile wurtzit ZnO yapısı elde edilmiştir. Sentez koşullarındaki farklılık ise ZnO yapılarının morfolojisini, kristal boyutunu ve yüzey alanını etkilemiştir. ZnO-F ve ZnO-R örneklerinin kristal boyutları sırasıyla 24,46 nm ve 31,10 nm olarak bulunmuştur. SEM analizi ile ZnO yapılarının morfolojisinde dikkate değer değişiklikler saptanmıştır. ZnO-F örneğinin yüzey alanı (20 m^2/g) ise ZnO-R örneğinin yüzey alanının (9,5 m^2/g) yaklaşık iki katıdır. XPS analizi ile ZnO yapılarının kimyasal halleri belirlenmiştir. Morfoloji ve reaksiyon koşullarının ZnO yapılarının foto aktivitesi üzerindeki etkisinin belirlenmesi Reaktif Kırmızı 194 (RR-194) boyasının degradasyonu ile incelenmiştir. Fotokatalitik aktivite deneylerinde ise ZnO-F katalizörünün ZnO-R katalizöründen daha iyi bir fotokatalitik performans sergilediği bulunmuştur.

Anahtar Kelimeler: Çiçek benzeri, hidrotermal yöntem, fotokataliz, fotokatalitik performans, Reaktif Kırmızı-194, çubuk benzeri, ZnO yapıları.

ToCite: TURKTEN, N. & KARATAS, Y., (2025). ZnO STRUCTURES: THE ROLE OF MORPHOLOGY IN PHOTOCATALYTIC DEGRADATION OF REACTIVE RED-194 DYE. *Kahramanmaraş Sütçü İmam Üniversitesi Mühendislik Bilimleri Dergisi*, 28(3), 1234-1245.

INTRODUCTION

Water pollution is a global problem caused by substantial industrial development and population growth. The textile industry is the most polluting sector globally with approximately 100 tons of dyes entering the wastewater system annually. Azo dyes are considered the most common class of colorants, representing over half of all industrial dyes. These dyes are highly soluble in water and difficult to remove or degrade due to their stability and aromatic molecular structure. The direct discharge of inadequately treated textile wastewater into the environment can cause severe health concerns to all living beings (Bhapkar and Bhame, 2024; Islam et al., 2023; Kumari et al., 2023; Saeed et al.,2022).

The removal of synthetic dyes is essential and can be accomplished through various primary water treatment strategies (Aksoy, 2024; Şentürk, 2024; Yıldız, 2024). Physical methods transfer pollutants from water to a solid phase medium without degrading them. Biological processes, on the other hand, often require a relatively prolonged treatment cycle. Advanced oxidation processes (AOPs) are well-known extremely effective water treatments that successfully decompose substances that are difficult to treat with conventional techniques. Among them, photocatalysis stands out as a prominent and environmentally friendly AOPs that minimizes secondary pollution. This method is notable for being simple, affordable, and capable of achieving complete oxidative mineralization of various pollutants (Bhapkar and Bhame, 2024; Islam et al., 2023; Saeed et al., 2022).

ZnO is a widely used economical and n-type semiconductor known for its exceptional photocatalytic properties in degrading organic pollutants in water. (Bhapkar and Bhame, 2024). The photocatalytic degradation mechanism of ZnO can be explained by reactions (1-7). The reaction is initiated after ZnO absorbs UV light (λ<390 nm) and indicates the generation of photogenerated electron/hole pairs (e^-/h^+). These charge carriers transfer into the ZnO leading to simultaneous redox reactions with surface-adsorbed O_2 that produce hydroxyl radicals ($\cdot OH$) and superoxide anions ($\cdot O_2^-$). The $\cdot O_2^-$ react with surface-adsorbed water to produce hydrogen peroxide (H_2O_2), which is responsible for the formation of $\cdot OH$ and they are possibly accountable for the degradation of most of the adsorbed organic pollutants, here RR-194 (Saikia et al., 2015).

$$ZnO + h\nu \rightarrow e^- + h^+ \quad (1)$$
$$e^- + O_2 \rightarrow \cdot O_2^- \quad (2)$$
$$\cdot O_2^- + e^- + 2H^+ \rightarrow H_2O_2 \quad (3)$$
$$H_2O_2 \rightarrow 2\ \cdot OH \quad (4)$$
$$h^+ + OH^- \rightarrow OH \quad (5)$$
$$h^+ + H_2O \rightarrow \cdot OH + H^+ \quad (6)$$
$$\cdot OH\ or\ \cdot O_2^- + pollutant_{ads} \rightarrow degraded\ product \quad (7)$$

Up to now, numerous synthetic approaches have been used to prepare special morphologies of ZnO structures (Ali et al., 2023; Das et al., 2019; Hussain et al., 2024; Lin et al., 2020; Sun et al., 2016). These approaches are mainly classified as physical and solution phase methods. Physical methods (thermal evaporation, chemical vapor deposition, etc.) are complex processes that proceed at high temperatures. The main drawback is the high operational costs, which limits its potential applications. On the other hand, the solution phase methods including sol-gel, hydrothermal, solvothermal, microemulsion, precipitation, etc. are widely applied processes that occur at low temperatures (<200 °C) (Ahmed et al., 2014; Raub et al., 2024; Shi et al., 2014). Amongst these methods, the hydrothermal method is a facile, cost-effective, and low-temperature process for fabricating various ZnO nanostructures. Additionally, the hydrothermal process provides precise control over nucleation, growth, aging rate, and uniformity, enabling effective particle size and morphology control. In this method, the alteration of reaction conditions such as precursor concentration, process time, pH, temperature, and solvents, results in different ZnO morphologies (Basnet and Chatterjee, 2020; Shi et al., 2014; H. Wang et al.,2011).

Recently, various strategies have been proposed to prepare one-dimensional (nanorods, wires, tubes, etc.), two-dimensional (nanosheets, nano pellets, etc.), and three-dimensional (coniferous urchin, flower, dandelion, etc.) ZnO nanostructures (Hahn, 2011; Sun et al., 2016; Xie et al.,2011). A variety of complex structural ZnO architectures such as hierarchical ZnO flower-rod arrays (Han et al., 2012), honeycomb Ag/ZnO heterostructures (Cai et al., 2013) have also been synthesized. One-dimensional and two-dimensional ZnO nanostructures exhibit a high surface-to-volume

ratio property. Three-dimensional hierarchical ZnO nanostructures are constructed from one-and/or two-dimensional ZnO blocks avoiding agglomerated configuration (Krishna et al., 2023; Lin et al., 2020; Zhu et al., 2018).

Several photocatalytic studies have reported on various morphological three-dimensional ZnO flower-like nanostructures and rod-like ZnO nanostructures synthesized by a hydrothermal process. Miao et al. prepared hydrangea-like and rose-like ZnO architectures, and the photocatalytic efficiency was tested on the degradation of Rhodamine B (RhB) (Miao et al., 2016). In addition, Zou et al. tested the photocatalytic activity of ZnO flower-like structures on RhB dye (Zou et al.,, 2022). In another study, one-dimensional ZnO structures exhibited a higher methylene blue (MB) degradation than three-dimensional flower-like ZnO structures (Lin et al., 2020). Duo et al. reported ultra-large ZnO macro flower particles and evaluated the photocatalytic activity of these nanoarchitectures on the photodegradation of MB dye (Duo et al., 2016). Kumaresan et al. prepared various morphological ZnO structures containing nanorods, hexagonal disks, and nanoflowers, and tested their photocatalytic activity on RhB (Kumaresan et al., 2017). Moreover, the photocatalytic of ZnO rod-like nanostructures was evaluated on the degradation of Reactive Yellow 15 (Hafez, 2012).

Herein, we reported the preparation of flower-like ZnO (ZnO-F) and rod-like ZnO (ZnO-R) via a hydrothermal process. These two special morphologies of ZnO structures were systematically characterized by FTIR, Raman spectroscopy, XRD, SEM, BET, and XPS analyses. This study also focused on the correlation between morphology and photocatalytic activity of structurally engineered ZnO specimens. The photocatalytic efficiency of ZnO structures was evaluated for the first time by testing their effectiveness in the degradation of RR-194 dye.

MATERIALS AND METHODS

Materials

Zinc acetate dihydrate ($Zn(CH_3COO)_2.2H_2O$, ACS reagent, ≥98%, Sigma-Aldrich, MW=219.51 g/mol) and ammonia solution 25% (NH_4OH, for analysis, Merck, MW=35.05 g/mol) were used in analyses.

Preparation of ZnO Structures

ZnO-F and ZnO-R structures were synthesized using zinc acetate as the precursor for ZnO structures. ZnO-F structures were prepared using a hydrothermal method proposed by Song and colleagues (Song et al., 2019). 0.02 mol zinc acetate was dissolved into 200 mL distilled water and placed in a flat-bottomed flask, and then 10 mL ammonia solution (25%) was added dropwise under magnetic stirring. The mixture was heated in a water bath pot at 80°C for 40 min. Then the cooled product was filtered, washed, dried at 80°C, and calcined at 500°C for 5 h. ZnO-R structures were prepared by a hydrothermal method described as followed with some modifications (Bhatti et al., 2019). 10 mL ammonia (25%) in a dropping funnel was added into 200 mL of 0.02 mol zinc acetate aqueous solution. After that, the beaker covered with aluminum foil was kept in an oven at 90°C for 6 h. Finally, the growth solid residue was filtered, washed, dried at 80°C, and calcined at 500°C for 5 h.

Characterization

Detailed information on characterization techniques were reported in detail in our previous work (Türkten and Karataş, 2024). Crystallite sizes (D, nm) of ZnO structures were calculated using the Scherrer equation (Equation (1)) related to (1 0 1) of the reflection plane of ZnO (Scherrer, 1918).

Photocatalytic Activity Experiments

The suspension (50 mL) was prepared by adding the optimum amount of photocatalyst (0.25 mg/L) in 10 mg/L RR-194 solution. The maximum wavelength of RR-194 was λ=522 nm. Detailed information on photocatalytic system was reported in our previous study (Türkten and Karataş, 2024). The percent removal of RR-194 dye was calculated using Equation (1).

$$\text{Decolorization, \%} = ((A_o - A) / A_o))x100 \quad (1)$$

where,
A_o: initial absorbance of RR-194 dye,
A_t: absorbance of RR-194 dye at time t.

RESULTS AND DISCUSSION

Characterization of ZnO Structures

FTIR spectra of ZnO-F and ZnO-R specimens are presented in Figure 1. For ZnO-F, the broad band around 3316 cm^{-1} corresponded to the stretching vibration of OH groups due to the hydroxyls or adsorbed water. The band around 2889 cm^{-1} was attributed to the C-H vibration mode. The observed bands at 1640 cm^{-1}, 1406 cm^{-1}, and 915 cm^{-1} belonged to asymmetric C=O stretching, symmetric C=O stretching, and C=O deformation mode of acetate groups, respectively. These zinc acetate groups could be adsorbed during the synthesis of ZnO structures. The signals below 1000 cm^{-1} in the fingerprint region corresponded to metal oxygen arising from inter-atomic vibrations. The observed metal oxide band at 562 cm^{-1} belonged to the Zn-O stretching (Janaki et al., 2015; Sharma et al., 2012). Compared to ZnO-F, the spectral band positions of ZnO-R were almost the same with slight shifts.

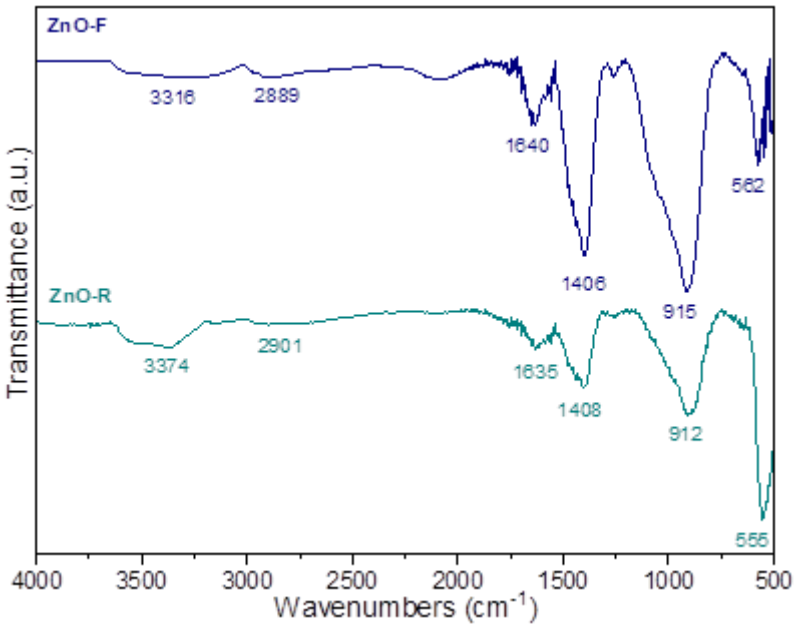

Figure 1. FTIR Spectra of ZnO-F and ZnO-R Structures.

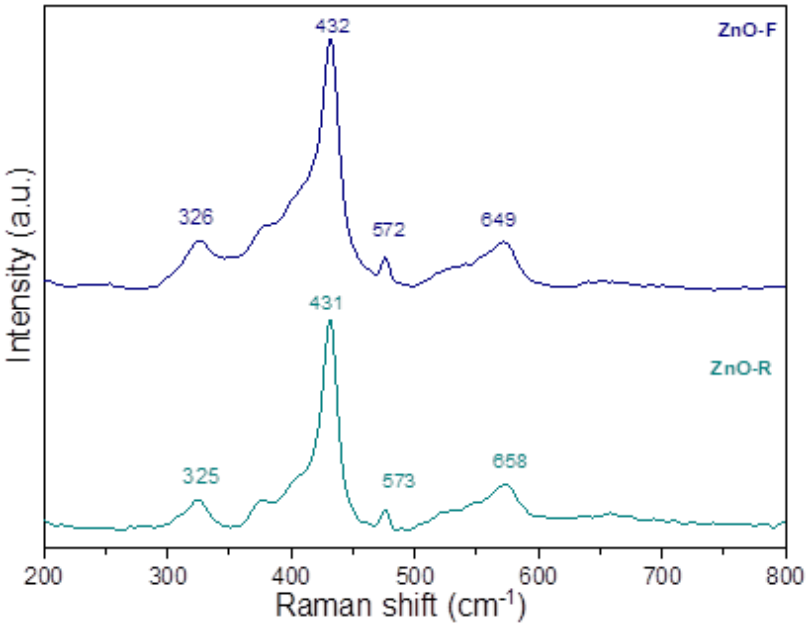

Figure 2. Raman Spectra of ZnO-F and ZnO-R Structures.

Raman features of ZnO-F and ZnO-R specimens are presented in Figure 2. The Raman spectrum of ZnO-F revealed an intense band at 432 cm^{-1} belonging to the E_2 (high) Raman mode and optical phonons for the wurtzite of ZnO. This mode was Raman active and non-polar, primarily attributed to the vibration of oxygen. The E_2 mode at 326 cm^{-1} was related to the second-order non-polar Raman process. The longitudinal optical phonons, E_1 (LO) mode at 572 cm^{-1} originated from impurities and/or defects such as oxygen vacancies. The wide band at 649 cm^{-1} could belong to the multiphonons process (Jung et al., 2012; Sharma et al., 2012; Zhang et al., 2009). It was noticed that the characteristic Raman bands of ZnO wurtzite also appeared in the spectrum of ZnO-R.

XRD diffractograms of ZnO-F and ZnO-R structures are presented in Figure 3. Both diffraction patterns were well-matched with the wurtzite type of ZnO (JCPDS No. 36-1451). For ZnO-F, the diffraction peaks at 2θ=31.80°, 34.46°, 36.30°, 47.54°, 56.62°, 62.90°, 66.38°, 67.96°, 69.08°, 72.60°, 76.90°, 81.36° corresponded to the (1 0 0), (0 0 2), (1 0 1), (1 0 2), (1 1 0), (1 0 3), (2 0 0), (1 1 2), (2 0 1), (0 0 4), (2 0 2) reflection planes of ZnO, respectively. Additionally, the XRD diffractogram of ZnO-R revealed sharper diffraction peaks than ZnO-F, indicating better crystallinity. The crystallite sizes of ZnO-F and ZnO-R specimens were 25 nm and 31 nm, respectively.

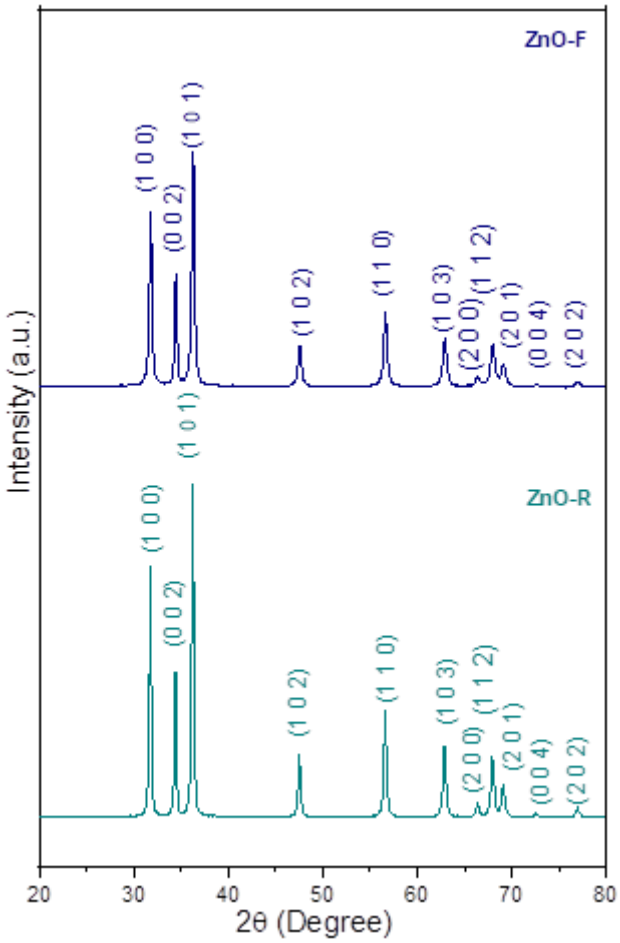

Figure 3. XRD Diffractograms of ZnO-F and ZnO-R Structures.

The morphological features of ZnO-F and ZnO-R specimens and the corresponding SEM images at three different magnifications (x20000, x50000, and x100000) are presented in Figure 4. ZnO-F specimen revealed a flower-like structure as expected with average lengths and thicknesses around 2 µm and 100-300 nm respectively. The flower structures were star-shaped with spikes radiating from the center. ZnO-R specimen was composed of thin rod-like particles with a length of around 2 µm. The type of hydrothermal process appears to influence the particle shape and particle size of ZnO.

(a)

(b)

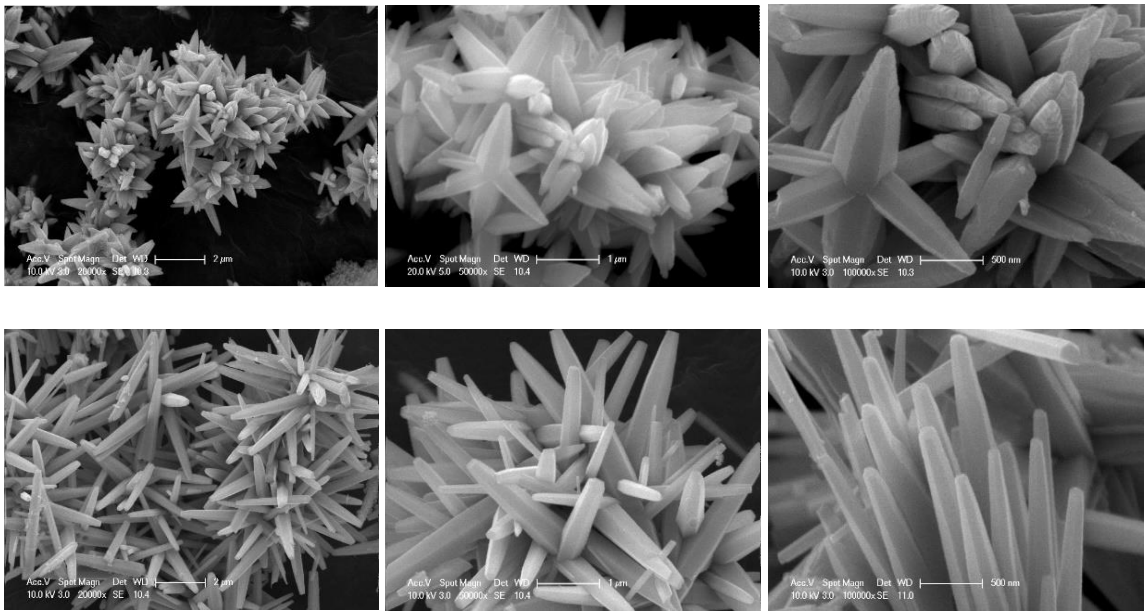

Figure 4. SEM Images of (a) ZnO-F and (b) ZnO-R ((left) x20000, (middle) x50000, (right) x100000).

According to the IUPAC classification (Sing, 1985), ZnO-F and ZnO-R specimens revealed a Type IV isotherm (Figure 5). The BET-specific surface areas of ZnO-F and ZnO-R specimens were calculated as 20 m^2/g and 10 m^2/g, respectively. It is important to note that the reaction conditions impact the surface area of ZnO. Rahimi and Yazdani reported that the ZnO nanorods prepared under ambient air exhibited a higher surface area (19.57 m^2/g) than the ZnO nanorods prepared under vacuum (15.44 m^2/g) (Rahimi and Yazdani, 2018). A similar low surface area (6.81 m^2/g and 7.2 m^2/g) was calculated for ZnO rods prepared by the sonochemical-assisted aqueous solution process (Mukhopadhyay et al., 2015). On the other hand, a high specific surface area (65.46 m^2/g) was obtained for ZnO nanorods synthesized via hydrothermal process (Sun and Park, 2022). Another study reported again a high surface area (269.86 m^2/g) for ZnO rod-like nanostructures (Hafez, 2012). Lin et al synthesized three-dimensional flowerlike ZnO nanostructures via hydrothermal method and reported an incredibly low BET surface area (1.77 m^2/g) (Lin et al., 2020). A similar surface area (4.58 m^2/g) was also observed for hydrothermally prepared ZnO flower-like nanostructures (Zou et al., 2022). Conversely, the surface area of ZnO-nanoflowers was reported as 17 m^2/g, which was similar to our findings (Lai et al., 2010). In addition, hydrangea-like ZnO and rose-like ZnO architectures were prepared via hydrothermal process, resulting in surface areas of 22.7 m^2/g and 37.3 m^2/g, respectively (Miao et al., 2016).

The pore diameter (D) and pore volume (V) values of ZnO-F and ZnO-R specimens are presented in Table 1. The pore sizes of both ZnO specimens were $20 Å < D < 500 Å$ and exhibited the characteristics of mesoporous structures (Sing, 1985). The dV/dD versus the pore diameter distribution curve of ZnO-F revealed the predominance of three types of mesopores was located at around $20 Å < D < 100 Å$. The two sharp peaks were centered at around 20 Å and 28 Å, whereas the distribution of larger mesopores with a broad peak centered at about 76 Å. For the ZnO-R specimen, a function of pore diameter distribution peaks was centered at around 28 Å, 50 Å, and 130 Å.

Table 1. BET Parameters of ZnO-F and ZnO-R Specimens

Specimens	Surface area (m^2/g)	Pore volume (cm^3/g)	Pore diameter (Å)
ZnO-F	20.02	0.0454	21.95
ZnO-R	9.464	0.0399	23.46

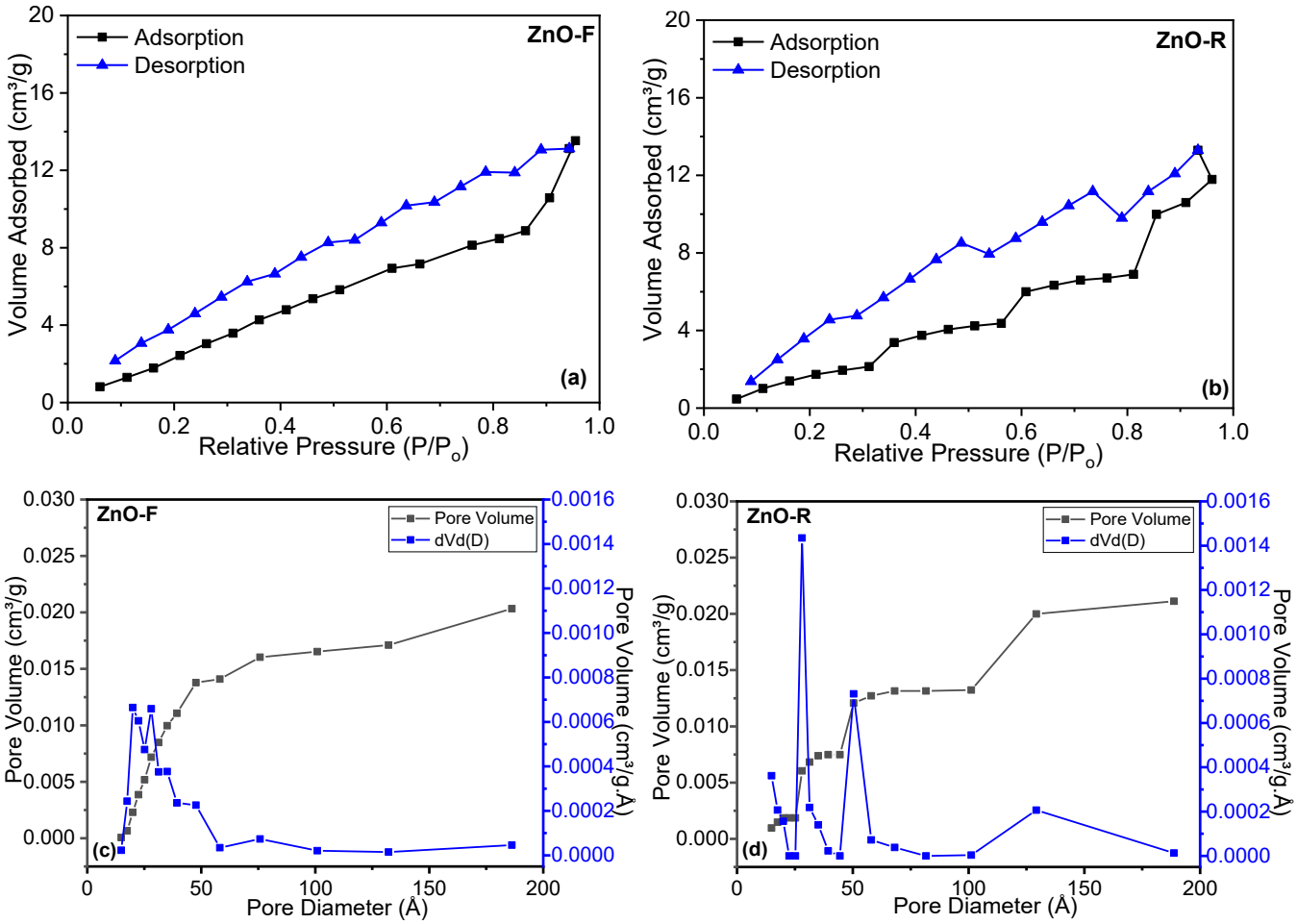

Figure 5. BET Adsorption/Desorption Isotherms (a) ZnO-F and (b) ZnO-R, and Pore Size Distribution Plots of (c) ZnO-F and (d) ZnO-R.

The survey scan spectra of ZnO specimens indicated the existence of Zn, O, and adventitious carbon (Figure 6 (a)). The detected carbon belonged to the residual acetate groups on the surface, which was exposed to the ambient atmosphere. The sharp peaks in binding energies of Zn $2p_{3/2}$, Zn $2p_{1/2}$, and O 1s corresponded to the core matrix elements of wurtzite ZnO (Batista-Grau et al., 2022). The Zn 2p core level spectra of ZnO-F and ZnO-R specimens exhibited a doublet Zn $2p_{3/2}$ and Zn $2p_{1/2}$, implying multicomponent Zn (Figure 6 (b)). The spectrum of the ZnO-F specimen signaled symmetric solitary peaks positioned at the binding energies of 1022.39eV and 1045.66 eV analogous to Zn $2p_{3/2}$ and Zn $2p_{1/2}$ core levels, respectively. A slight position shift in binding energies of Zn $2p_{3/2}$ (1022.09 eV) and Zn $2p_{1/2}$ (1045.01 eV) peaks for the ZnO-R specimen was observed. The difference between Zn $2p_{3/2}$ and Zn $2p_{1/2}$ peak positions was ΔE=23.27 eV and ΔE=22.92 eV for ZnO-F and ZnO-R specimens, respectively. The energy level separation between two core-level Zn components was consistent with literature values for ZnO, indicating that the zinc ions (Zn) could be in a divalent (2+) oxidation state (Moulder and Chastain, 1992).

The deconvoluted O 1s spectra of ZnO-F (Figure 6 (c)) and ZnO-R (Figure 6 (d)) were divided into three peaks. The lower binding energies of ZnO-F and ZnO-R were observed at 530.2 eV and 530.7 eV, respectively, corresponding to the wurtzite structure of the hexagonal Zn^{2+} ion of ZnO. These peaks could be related to Zn–O bonds. The medium binding energies of ZnO-F (531.19 eV) and ZnO-R (531.37 eV) components were attributed to the oxygen vacancies or defects belonging to O_2^- ions within the oxygen-deficient regions of the ZnO matrix. The intensity variations of this component could be related to the concentration of oxygen vacancies and this peak was particularly intense in the ZnO-F specimen. The O1s peaks at 532.33 eV and 532.34 eV for the ZnO-F and ZnO-R specimens, respectively, mainly belonged to a loosely bound oxygen. These peaks especially could be related to chemisorbed or dissociated oxygen species, i.e. Zn–OH and H_2O, which were intensely correlated with surface disorders on ZnO (Batista-Grau et al., 2022; Das et al., 2010; Wang et al., 2012).

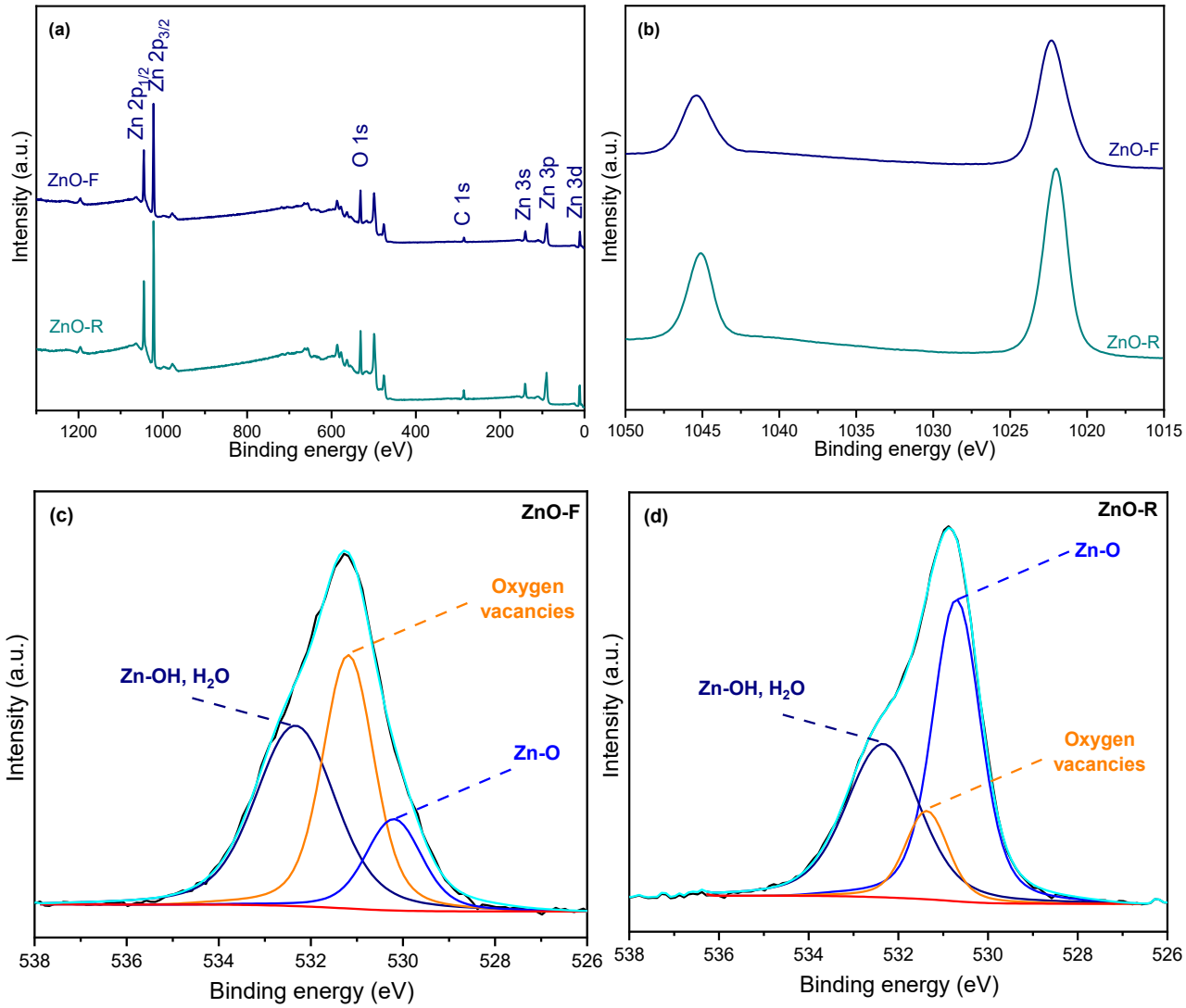

Figure 6. XPS Spectra of ZnO-F and ZnO-R Structures (a) All Survey Spectra, (b) Zn 2p, (c, d) the O 1s Deconvoluted Spectra.

Photocatalytic Activity of ZnO Structures

The photocatalytic activities of ZnO-F and ZnO-R specimens on RR-194 degradation were investigated (Figure 7) and followed pseudo first-order kinetic model (Table 2).

The removal efficiencies of RR-194 were 32% and 21% for ZnO-F and ZnO-R, respectively. The efficiency of ZnO-F is comparatively high, which may be related to the concentration of oxygen vacancies in specimens, as confirmed by XPS. Oxygen vacancies can serve as electron traps, hindering the recombination of electron-hole pairs and leading to changes in light absorption capacity and photocatalytic activity (Wang et al., 2012). Moreover, oxygen vacancies can create active species, and capture the photoinduced electrons, thereby enhancing the efficiency of dye photodegradation (Han et al., 2012).

Table 2. Photocatalytic Degradation Kinetics of RR-194

	First-order kinetic parameters		
	$kx10^{-4}$ (min^{-1})	**$t_{1/2}$ (min)**	**$Ratex10^{-4}$ (cm^{-1} min^{-1})**
ZnO-F	6.42	1080	1.12
ZnO-R	3.95	1756	0.687

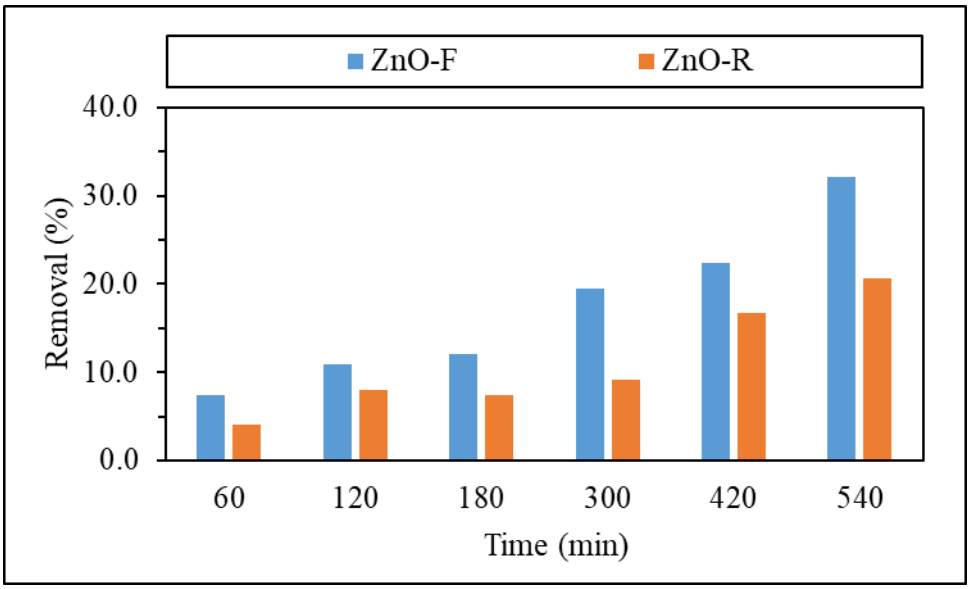

Figure 7. Removal Efficiencies of ZnO-F and ZnO-R Structures.

The ZnO-F specimen revealed a higher photocatalytic activity in RR-194 degradation compared to ZnO-R. The calculated rate constants of ZnO-F and ZnO-R were $k=6.42x10^{-4}$ min^{-1} and $k=3.95x10^{-4}$ min^{-1}, respectively. The surface area of the ZnO-F specimen (ca. 20 m^2/g) was twice as large as that of the ZnO-R specimen (ca. 9.5 m^2/g). It is well established that a greater surface area increases the interaction between the pollutant and the photocatalyst, offering more functional sites for photocatalytic reactions (Kim et al.,2007; Zou et al., 2022). Zou et al. reported that the flower-like nanostructures of ZnO, assembled from nanosheets, exhibited superior photocatalytic performance compared to those formed from nanorods. This enhanced performance in the degradation of RhB could be attributed to the larger specific surface area and a greater number of OH groups adsorbed on the catalyst surfaces (Zou et al., 2022). Another study reported the affirmative effect of a large surface area on the photocatalytic performance of ZnO structures (Miao et al., 2016). Moreover, the crystallite size of the catalyst influences photocatalytic activity. According to XRD results, the ZnO-F specimen (25 nm) exhibited a lower crystallite size than the ZnO-R specimen (31 nm). Based on the existing literature, crystallite size, oxygen vacancies, and surface area are the factors that impact photocatalytic performance interdependently (Han et al., 2012; Kim et al., 2007; Miao et al., 2016; Wang et al., 2012). These findings are consistent with our photocatalytic experimental results.

CONCLUSION

In the study, ZnO-F and ZnO-R structures were synthesized by a simple hydrothermal method. different synthesis routes in the hydrothermal preparation processes resulted in two distinct morphologies of ZnO structures, exhibiting varying surface areas and crystallite sizes. XRD and Raman confirmed that both specimens exhibited the wurtzite structure of ZnO. The photocatalytic activity increased as crystallite size decreased, and surface area increased. SEM, XRD, XPS, and BET analysis indicated that the differences in morphology, surface area, oxygen vacancies, and crystallite size affected the photocatalytic performance of ZnO structures. The ZnO-F specimen revealed higher efficiency in the photocatalytic degradation of RR-194 than the ZnO-R specimen. Advances in the designing of ZnO structures to enhance their photocatalytic performance would make them promising candidates for water treatment, highlighting the necessity to direct further research and development in this field.

Funding: This work was supported by Research Fund of Kirsehir Ahi Evran University through Project FEF.A4.22.008.

REFERENCES

Ahmed, F., Arshi, N., Anwar, M. S., Danish, R., & Koo, B. H. (2014). Morphological evolution of ZnO nanostructures and their aspect ratio-induced enhancement in photocatalytic properties. *RSC Advances, 4*(55), 29249-29263. doi:10.1039/C4RA02470B

Aksoy, Y. (2024). Direct Hf Etching-Derived Ti3c2tx: A Potent Adsorbent for Basic Red 46 Dye. *Kahramanmaraş Sütçü İmam Üniversitesi Mühendislik Bilimleri Dergisi*, 27(4), 1571-1581. https://doi.org/10.17780/ksujes.1500888

Ali, J., Bibi, S., Jatoi, W. B., Tuzen, M., Jakhrani, M. A., Feng, X., & Saleh, T. A. (2023). Green synthesized zinc oxide nanostructures and their applications in dye-sensitized solar cells and photocatalysis: A review. *Materials Today Communications, 36*, 106840. doi:https://doi.org/10.1016/j.mtcomm.2023.106840

Basnet, P., & Chatterjee, S. (2020). Structure-directing property and growth mechanism induced by capping agents in nanostructured ZnO during hydrothermal synthesis—A systematic review. *Nano-Structures & Nano-Objects, 22*, 100426. doi:https://doi.org/10.1016/j.nanoso.2020.100426

Batista-Grau, P., Fernández-Domene, R. M., Sánchez-Tovar, R., Blasco-Tamarit, E., Solsona, B., & García-Antón, J. (2022). Indirect charge transfer of holes via surface states in ZnO nanowires for photoelectrocatalytic applications. *Ceramics International, 48*(15), 21856-21867. doi:https://doi.org/10.1016/j.ceramint.2022.04.170

Bhapkar, A. R., & Bhame, S. (2024). A review on ZnO and its modifications for photocatalytic degradation of prominent textile effluents: Synthesis, mechanisms, and future directions. *Journal of Environmental Chemical Engineering, 12*(3), 112553. doi:https://doi.org/10.1016/j.jece.2024.112553

Bhatti, M. A., Shah, A. A., Almani, K. F., Tahira, A., Chalangar, S. E., Chandio, A. d., . . . Ibupoto, Z. H. (2019). Efficient photo catalysts based on silver doped ZnO nanorods for the photo degradation of methyl orange. *Ceramics International, 45*(17), 23289-23297. doi:10.1016/j.ceramint.2019.08.027

Cai, Y., Fan, H., Xu, M., & Li, Q. (2013). Rapid photocatalytic activity and honeycomb Ag/ZnO heterostructures via solution combustion synthesis. *Colloids and Surfaces A: Physicochemical and Engineering Aspects, 436*, 787-795. doi:https://doi.org/10.1016/j.colsurfa.2013.08.008

Das, A., S.K, N., & Nair, R. G. (2019). Influence of surface morphology on photocatalytic performance of zinc oxide: A review. *Nano-Structures & Nano-Objects, 19*, 100353. doi:https://doi.org/10.1016/j.nanoso.2019.100353

Das, J., Pradhan, S. K., Sahu, D. R., Mishra, D. K., Sarangi, S. N., Nayak, B. B.,Verma, S., & Roul, B. K. (2010). Micro-Raman and XPS studies of pure ZnO ceramics. *Physica B: Condensed Matter, 405*(10), 2492-2497. doi:https://doi.org/10.1016/j.physb.2010.03.020

Duo, S., Li, Y., Liu, Z., Zhong, R., & Liu, T. (2016). Novel hybrid self-assembly of an ultralarge ZnO macroflower and defect intensity-induced photocurrent and photocatalytic properties by facile hydrothermal synthesis using CO(NH2)2–N2H4 as alkali sources. *Materials Science in Semiconductor Processing, 56*, 196-212. doi:https://doi.org/10.1016/j.mssp.2016.08.018

Hafez, H. S. (2012). Highly active ZnO rod-like nanomaterials: Synthesis, characterization and photocatalytic activity for dye removal. *Physica E: Low-dimensional Systems and Nanostructures, 44*(7), 1522-1527. doi:https://doi.org/10.1016/j.physe.2012.03.020

Hahn, Y.-B. (2011). Zinc oxide nanostructures and their applications. *Korean Journal of Chemical Engineering, 28*(9), 1797-1813. doi:10.1007/s11814-011-0213-3

Han, Z., Liao, L., Wu, Y., Pan, H., Shen, S., & Chen, J. (2012). Synthesis and photocatalytic application of oriented hierarchical ZnO flower-rod architectures. *Journal of Hazardous materials, 217-218*, 100-106. doi:https://doi.org/10.1016/j.jhazmat.2012.02.074

Hussain, R. T., Hossain, M. S., & Shariffuddin, J. H. (2024). Green synthesis and photocatalytic insights: A review of zinc oxide nanoparticles in wastewater treatment. *Materials Today Sustainability, 26*, 100764. doi:https://doi.org/10.1016/j.mtsust.2024.100764

Islam, M., Kumar, S., Saxena, N., & Nafees, A. (2023). Photocatalytic Degradation of Dyes Present in Industrial Effluents: A Review. *ChemistrySelect, 8*(26), e202301048. doi:https://doi.org/10.1002/slct.202301048

Janaki, A. C., Sailatha, E., & Gunasekaran, S. (2015). Synthesis, characteristics and antimicrobial activity of ZnO nanoparticles. *Spectrochimica Acta Part A: Molecular and Biomolecular Spectroscopy, 144*, 17-22. doi:https://doi.org/10.1016/j.saa.2015.02.041

Jung, H. J., Lee, S., Yu, Y., Hong, S. M., Choi, H. C., & Choi, M. Y. (2012). Low-temperature hydrothermal growth of ZnO nanorods on sol–gel prepared ZnO seed layers: Optimal growth conditions. *Thin Solid Films, 524*, 144-150. doi:https://doi.org/10.1016/j.tsf.2012.10.007

Kim, D. S., Han, S. J., & Kwak, S.-Y. (2007). Synthesis and photocatalytic activity of mesoporous TiO_2 with the surface area, crystallite size, and pore size. *Journal of Colloid and Interface Science, 316*(1), 85-91. doi:https://doi.org/10.1016/j.jcis.2007.07.037

Krishna, M. S., Singh, S., Batool, M., Fahmy, H. M., Seku, K., Shalan, A. E., . . . Zafar, M. N. (2023). A review on 2D-ZnO nanostructure based biosensors: from materials to devices. *Materials Advances, 4*(2), 320-354. doi:10.1039/D2MA00878E

Kumaresan, N., Ramamurthi, K., Ramesh Babu, R., Sethuraman, K., & Moorthy Babu, S. (2017). Hydrothermally grown ZnO nanoparticles for effective photocatalytic activity. *Applied Surface Science, 418*, 138-146. doi:https://doi.org/10.1016/j.apsusc.2016.12.231

Kumari, H., Sonia, Suman, Ranga, R., Chahal, S., Devi, S., . . . Parmar, R. (2023). A Review on Photocatalysis Used For Wastewater Treatment: Dye Degradation. *Water, Air, & Soil Pollution, 234*(6), 349. doi:10.1007/s11270-023-06359-9

Lai, Y., Meng, M., & Yu, Y. (2010). One-step synthesis, characterizations and mechanistic study of nanosheets-constructed fluffy ZnO and Ag/ZnO spheres used for Rhodamine B photodegradation. *Applied Catalysis B: Environmental, 100*(3), 491-501. doi:https://doi.org/10.1016/j.apcatb.2010.08.027

Lin, Y., Hu, H., & Hu, Y. H. (2020). Role of ZnO morphology in its reduction and photocatalysis. *Applied Surface Science, 502*, 144202. doi:https://doi.org/10.1016/j.apsusc.2019.144202

Miao, Y., Zhang, H., Yuan, S., Jiao, Z., & Zhu, X. (2016). Preparation of flower-like ZnO architectures assembled with nanosheets for enhanced photocatalytic activity. *Journal of Colloid and Interface Science, 462*, 9-18. doi:https://doi.org/10.1016/j.jcis.2015.09.064

Moulder, J. F., & Chastain, J. (1992). *Handbook of X-ray Photoelectron Spectroscopy: A Reference Book of Standard Spectra for Identification and Interpretation of XPS Data*: Physical Electronics Division, Perkin-Elmer Corporation.

Mukhopadhyay, S., Das, P. P., Maity, S., Ghosh, P., & Devi, P. S. (2015). Solution grown ZnO rods: Synthesis, characterization and defect mediated photocatalytic activity. *Applied Catalysis B: Environmental, 165*, 128-138. doi:https://doi.org/10.1016/j.apcatb.2014.09.045

Rahimi, K., & Yazdani, A. (2018). Improving photocatalytic activity of ZnO nanorods: A comparison between thermal decomposition of zinc acetate under vacuum and in ambient air. *Materials Science in Semiconductor Processing, 80*, 38-43. doi:https://doi.org/10.1016/j.mssp.2018.02.018

Raub, A. A. M., Bahru, R., Nashruddin, S. N. A. M., & Yunas, J. (2024). A review on vertical aligned zinc oxide nanorods: Synthesis methods, properties, and applications. *Journal of Nanoparticle Research, 26*(8), 186. doi:10.1007/s11051-024-06098-w

Saeed, M., Muneer, M., Haq, A. u., & Akram, N. (2022). Photocatalysis: an effective tool for photodegradation of dyes—a review. *Environmental Science and Pollution Research, 29*(1), 293-311. doi:10.1007/s11356-021-16389-7

Saikia, L., Bhuyan, D., Saikia, M., Malakar, B., Dutta, D. K., & Sengupta, P. (2015). Photocatalytic performance of ZnO nanomaterials for self sensitized degradation of malachite green dye under solar light. *Applied Catalysis A: General, 490*, 42-49. doi:https://doi.org/10.1016/j.apcata.2014.10.053

Scherrer, P. (1918). Estimation of the size and internal structure of colloidal particles by means of röntgen. *Nachrichten von der Gesellschaft der Wissenschaften zu Göttingen, 2*, 96–100.

Sharma, A., Singh, B. P., Dhar, S., Gondorf, A., & Spasova, M. (2012). Effect of surface groups on the luminescence property of ZnO nanoparticles synthesized by sol–gel route. *Surface Science, 606*(3), L13-L17. doi:https://doi.org/10.1016/j.susc.2011.09.006

Shi, L.-E., Li, Z.-H., Zheng, W., Zhao, Y.-F., Jin, Y.-F., & Tang, Z.-X. (2014). Synthesis, antibacterial activity, antibacterial mechanism and food applications of ZnO nanoparticles: a review. *Food Additives & Contaminants: Part A, 31*(2), 173-186. doi:10.1080/19440049.2013.865147

Sing, K. S. W. (1985). Reporting physisorption data for gas/solid systems with special reference to the determination of surface area and porosity (Recommendations 1984). *Pure and Applied Chemistry, 57*(4), 603-619. doi:doi:10.1351/pac198557040603

Song, Z., Chen, W., Zhang, H., Li, Y., Zeng, W., Tang, S., & Zhu, C. (2019). Highly sensitive and selective acetylene sensors based on p-n heterojunction of NiO nanoparticles on flower-like ZnO structures. *Ceramics International, 45*(16), 19635-19643. doi:https://doi.org/10.1016/j.ceramint.2019.06.212

Sun, H., & Park, S.-J. (2022). Highly efficient reduction of aqueous Cr(VI) with novel ZnO/SnS nanocomposites through the piezoelectric effect. *Journal of Environmental Sciences, 118*, 57-66. doi:https://doi.org/10.1016/j.jes.2021.08.023

Sun, Y., Chen, L., Bao, Y., Zhang, Y., Wang, J., Fu, M., Wu, J.,& Ye, D. (2016). The Applications of Morphology Controlled ZnO in Catalysis. *Catalysts, 6*(12), 188. Retrieved from https://www.mdpi.com/2073-4344/6/12/188

Şentürk, İ. (2024). Sentezlenen Metal Oksit Nanokompozit Yardımıyla Sucul Çözeltilerden Reaktif Azo Boya Giderimi. *Kahramanmaraş Sütçü İmam Üniversitesi Mühendislik Bilimleri Dergisi*, 27(2), 523-538. https://doi.org/10.17780/ksujes.1403697

Türkten, N., & Karataş, Y. (2024). A Novel Study On The Synthesis, Characterization, and Photocatalytic Activity of CeO_2 Nanoparticles. *Kahramanmaraş Sütçü İmam Üniversitesi Mühendislik Bilimleri Dergisi, 27*(1), 190-198. doi:10.17780/ksujes.1369994

Wang, H., Xie, J., Yan, K., & Duan, M. (2011). Growth Mechanism of Different Morphologies of ZnO Crystals Prepared by Hydrothermal Method. *Journal of Materials Science & Technology, 27*(2), 153-158. doi:https://doi.org/10.1016/S1005-0302(11)60041-8

Wang, J., Wang, Z., Huang, B., Ma, Y., Liu, Y., Qin, X., Zhang, X., & Dai, Y. (2012). Oxygen Vacancy Induced Band-Gap Narrowing and Enhanced Visible Light Photocatalytic Activity of ZnO. *ACS Applied Materials & Interfaces, 4*(8), 4024-4030. doi:10.1021/am300835p

Xie, J., Li, Y., Zhao, W., Bian, L., & Wei, Y. (2011). Simple fabrication and photocatalytic activity of ZnO particles with different morphologies. *Powder Technology, 207*(1), 140-144. doi:https://doi.org/10.1016/j.powtec.2010.10.019

Yıldız, H. (2024). Atıksudan Boya Giderimindeki Gelişmeler: Adsorpsiyon Teknolojisi ve Geleceğe Yönelik Beklentiler. *Kahramanmaraş Sütçü İmam Üniversitesi Mühendislik Bilimleri Dergisi*, 27(4), 1544-1556. https://doi.org/10.17780/ksujes.1470859

Zhang, R., Yin, P.-G., Wang, N., & Guo, L. (2009). Photoluminescence and Raman scattering of ZnO nanorods. *Solid State Sciences, 11*(4), 865-869. doi:https://doi.org/10.1016/j.solidstatesciences.2008.10.016

Zhu, L., Li, Y., & Zeng, W. (2018). Hydrothermal synthesis of hierarchical flower-like ZnO nanostructure and its enhanced ethanol gas-sensing properties. *Applied Surface Science, 427*, 281-287. doi:https://doi.org/10.1016/j.apsusc.2017.08.229

Zou, X., Ke, J., Hao, J., Yan, X., & Tian, Y. (2022). A new method for synthesis of ZnO flower-like nanostructures and their photocatalytic performance. *Physica B: Condensed Matter, 624*, 413395. doi:https://doi.org/10.1016/j.physb.2021.413395